A SIMPLIFIED MODEL OF FRACKING BASED ON THE TOPOLOGICAL DERIVATIVE CONCEPT

M. XAVIER, N. VAN GOETHEM AND A.A. NOVOTNY

Abstract. This paper deals with a simplified hydraulic fracture model based on the concept of topological derivatives. It means that we consider a two dimensional idealization in which the rock is assumed to be impermeable, while the fracturing process is activated by a given pressure acting within the existing geological faults. The basic idea consists in adapting the Francfort-Marigo damage model to the context of hydraulic fracture. The Francfort-Marigo damage model is a variational approach to describe the behavior of brittle materials under the quasi-static loading assumption, focusing on the evolution of damaged regions under an irreversibility constraint. In our model problem, the loading comes out from a pressurized damaged region embedded into the rock, which is used to trigger the hydraulic fracturing process. In particular, a shape functional given by the sum of the total potential energy of the system with a Griffith-type dissipation energy term is minimized with respect to a set of ball-shaped pressurized inclusions by using the topological derivative concept. Thus, the topological asymptotic expansion of the shape functional with respect to the nucleation of a circular inclusion endowed with non-homogeneous transmission condition on its boundary is obtained. The associated topological derivative, which corroborates with the famous Eshelby theorem, is used to devise a simple topology optimization algorithm specifically designed to simulate the whole nucleation and propagation process of hydraulic fracturing. To assess our model, some numerical examples are presented, showing typical features of hydraulic fracture phenomenon, including the characterization of the fault-activation pressure and specific crack path growth, allowing for kinking and bifurcations.

1. Introduction

Hydraulic fracturing is an industrial process that requires to pump a mixture of water, proppant (usually sand), and some chemical additives into layers of rock and shale. The purpose is to create and/or extend cracks from some pre-existing geological faults in order to let the gas that was trapped into the rocks be extracted at the surface. Roughly speaking, the process starts by perforating a vertical well into the reservoir. As soon as the required depth is reached, the perforation continues in the horizontal direction. Finally, the pumping mechanism of the aforementioned mixture at an extremely high pressure is launched. Then, the pressure inside the damaged region is increased until a critical value is attained at which fault-activation is triggered.

The hydraulic fracturing process is nowadays very much debated, since in its current form it is extremely damageable for the ecosystem. In particular, it is currently forbidden in Europe and many regions of the world, including Brazil, since an uncontrolled use of this technique leads to severe environmental issues. The first is water consumption: in 2010, the U.S. Environmental Protection Agency estimated that 300 to 500 million cubic meters of water are used to fracture 35.000 wells in the United States each year. The extraction of so much water for fracking has raised concerns about the ecological impacts to aquatic resources, as well as dewatering of drinking water aquifers. A second dramatic issue is the fact that shale gas wells can use more than 2 million kilograms of proppant per well, that is, about 5 times more than alternative oil extraction techniques.

Key words and phrases. Hydraulic fracture modelling, Francfort-Marigo damage model, topological derivative, topology optimization algorithm.

Furthermore, in addition to large volumes of water, a variety of chemicals are used in hydraulic fracturing fluids, typically of the order of 0.5% and 2.0% of the total volume of the fracturing fluid, which represents huge quantities in respect of the enormous volume of water used[1]. It is therefore of major importance to be able to numerically simulate any such shale gas extraction technique, in order to anticipate the risks, monitorate and optimize the industrial process.

However, the *real world* hydraulic fracturing process (fracking) is a purely three dimensional and very complex phenomenon (Secchi and Schrefler, 2012; Salimzadeh et al., 2017). Therefore, some *ad hoc* simplifications are here introduced. The reservoir is assumed to be composed by a horizontal pressurization well and the region to be fractured. In addition, it is supposed that the fracture pattern is periodic. Then, a single block of the reservoir is taken as reference domain to represent the whole fracture network. Finally, we consider a two dimensional idealization in which the rock is assumed to be impermeable, while the fracturing process is activated by a given pressure acting within the existing geological faults. Therefore, fluid-structure interaction phenomenon is not considered in our model. See sketch in Figure 1.

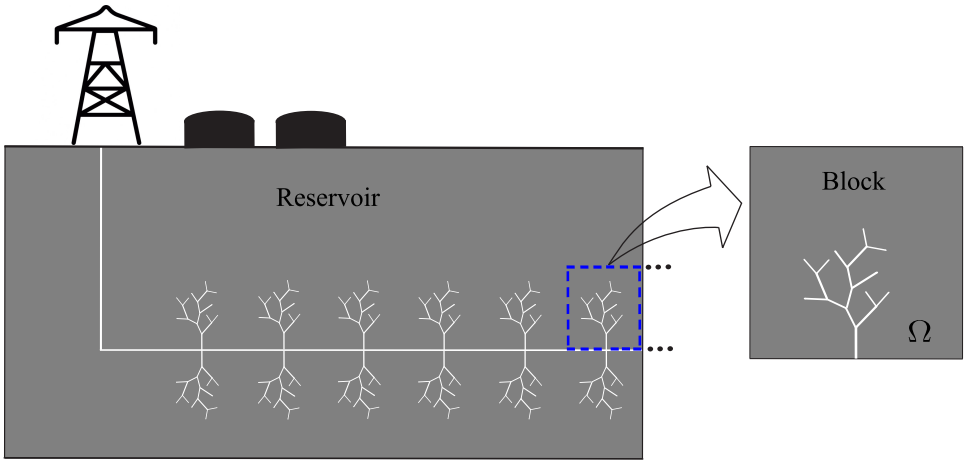

FIGURE 1. Fractured reservoir.

In this simplified context, the present paper proposes a novel hydraulic fracture model based on the topological derivative concept. The basic idea consists in adapting the Francfort-Marigo damage model (Francfort and Marigo, 1993) to the context of hydraulic fracturing phenomenon. The Francfort-Marigo damage model describes the behavior of brittle materials under the quasi-static loading assumption, focusing on the evolution of damaged regions under an irreversibility constraint. Such a model has been successfully applied to simulate fracturing process in brittle materials, where the crack is identified with a thin damage (Bourdin et al., 2000, 2008). See also recent papers by Allaire et al. (2011) and Xavier et al. (2017) where the topological derivative concept is incorporated to the Francfort-Marigo model. According to our assumptions, the loading comes out from a prescribed pressure inside the damaged region, which is used to trigger the hydraulic fracturing process. In particular, a shape functional given by the sum of the total potential energy of the system with a Griffith-type dissipation energy term is minimized with respect to a set of ball-shaped pressurized inclusions by using the topological derivative concept (Novotny and Sokołowski, 2013; Sokołowski and Żochowski, 1999). More precisely, the topological asymptotic expansion of the shape functional, taking into account

[1]See https://www.earthworksaction.org/issues/detail/hydraulic_fracturing_101#.WRluRDe1tpg

the nucleation of a circular inclusion endowed with non-homogeneous transmission condition on its boundary, is obtained. It is observed that the associated topological derivative fits the famous Eshelby theorem (Eshelby, 1957, 1959) which represents one of the major advances in the continuum mechanics theory of the 20$^{\text{th}}$ century (Kachanov et al., 2003). The obtained topological derivative is used as descent direction to minimize the proposed shape functional indicating the regions that have to be damaged. Based on this natural idea, a simple topology optimization algorithm specifically designed to simulate the whole nucleation and propagation hydraulic fracturing process is devised. Finally, some numerical examples are presented, showing important features associated with hydraulic fracture phenomenon, including the characterization of the fault-activation pressure and crack path growth, allowing for kinking and bifurcations. In our simplified setting the pressure increases monotonically, so that it may represent a high viscosity fluid pumping under very low injection rate (L'homme et al., 2002), for instance. However, it is well known that pressure oscillations may appear during the fracking process (Zhang and Chen, 2010; Soliman et al., 2014; Feng and Gray, 2017). The reader interested in more sophisticated approaches dealing with realistic hydraulic fracture phenomenon may refer to Kim and Moridis (2015), Milanese et al. (2016) and Cao et al. (2017), for instance.

The paper is organized as follows. The hydraulic fracture mechanical model is introduced in Section 2. Section 3 shows the closed form for the associated topological derivative. In Section 4 the resulting topology optimization algorithm is presented in details. A set of numerical experiments are driven in Section 5. Finally, some concluding remarks are presented in Section 6.

2. A simplified model of fracking

In this section we present the main aspects concerning Francfort-Marigo damage model together with its adapted version to the context of hydraulic fracture phenomenon. As already mentioned, the whole fracture network is represented by a single block into two spatial dimensions. The rock is assumed to be impermeable and the loading comes out from a given pressure acting within the damaged region, so that fluid-structure interaction phenomenon is not taken into account. In addition, body forces are neglected, allowing for focus on the influence of the internal pressure only.

2.1. **Francfort-Marigo damage model.**

Damage models, like the one introduced by Francfort-Marigo, initially propose that a damaged elastic body is composed by two distinct materials. To introduce this idea, let us consider an open and bounded domain $\Omega \subset \mathbb{R}^2$ with Lipschitz boundary $\partial\Omega$ and a sub-domain ω of the form $\omega \subset \Omega$, see Figure 2. Then, a parameter ρ, defined as

$$\rho = \rho(x) := \begin{cases} 1, & \text{if } x \in \Omega \setminus \overline{\omega}\,, \\ \rho_0, & \text{if } x \in \omega\,, \end{cases} \tag{2.1}$$

with $0 < \rho_0 \ll 1$, is introduced to characterize the damage distribution. Therefore, the region $\Omega \setminus \overline{\omega}$ represents the healthy part of the domain, while ω represents the damaged region.

The change from the original material to the damaged one occurs only if the elastic energy released by this transition overcomes a certain material-dependent threshold. In other words, the occurrence of new damage is determined by the relation

$$\frac{1}{2}\mathbb{C}\epsilon \cdot \epsilon - \frac{1}{2}\rho_0 \mathbb{C}\epsilon \cdot \epsilon > \kappa\,, \tag{2.2}$$

where $\mathbb{C}$ is the fourth-order elasticity tensor, ϵ is the second-order strain tensor and κ is a material property that represents the damage toughness.

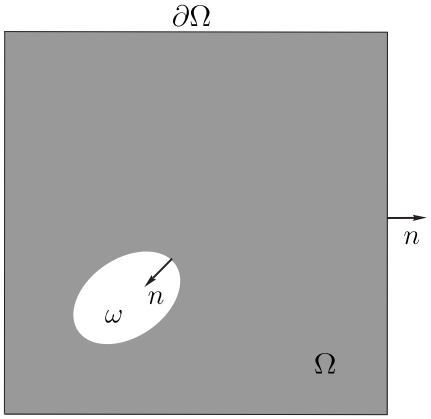

FIGURE 2. Unperturbed problem.

Finally, the model proposes a shape functional, $\mathcal{F}_\omega(u_i)$, to be minimized at each time step t_i, defined as

$$\mathcal{F}_\omega(u_i) = \mathcal{J}(u_i) + \kappa|\omega| \,, \tag{2.3}$$

where u_i is the displacement field at the time t_i and $|\omega|$ is the Lebesgue measure of ω. As mentioned, the first term on the right side of (2.3) represents the total potential energy of the system while the second term is the so called Griffith-type dissipation energy.

In addition, two conditions are assumed in this model. The first one considers that the healthy material should be stiffer than the damaged phase to characterize the stiffness loss associated to the crack growth. The second condition ensures that the fracturing process is irreversible, which means that healing is precluded. For a complete description of the Francfort-Marigo damage model see the original paper by Francfort and Marigo (1993).

2.2. **Mechanical model of hydraulic fracture.** Now, in order to adapt the Francfort-Marigo model to the context of hydraulic fracture it is considered that the damaged region ω is submitted to some internal pressure. By this way, a normal force is applied on the damage front $\partial\omega$. In addition, the pressure inside the damaged region ω, depending on the time instant t_i, is given by

$$p_i = p_{i-1} + \Delta p_i \,, \tag{2.4}$$

where Δp_i is the pressure increment. Therefore, the total applied pressure p is computed as the sum

$$p = p_0 + \sum_{i=1}^{N} \Delta p_i \,, \tag{2.5}$$

where p_0 is the initial pressure and N the total number of increments. Note that for each incremental pressure p_i a new displacement field u_i is induced. Then, in order to simplify future notations the subscript i in the displacement field u_i will be omitted.

Therefore, the hydraulic fracture model has the same structure of Francfort-Marigo model and, in particular, relies on the following shape functional:

$$\mathcal{F}_\omega(u) = \mathcal{J}(u) + \kappa|\omega| \,, \tag{2.6}$$

where the total potential energy $\mathcal{J}(u)$ is given by

$$\mathcal{J}(u) = \frac{1}{2}\int_\Omega \sigma(u) \cdot \nabla u^s dx - \int_\omega p_i \,\mathrm{div}(u) dx \,, \tag{2.7}$$

where p_i is the current pressure assumed to be constant in $\omega \subset \Omega$. The vector function u is solution to the following variational problem: Find $u \in \mathcal{U}$, such that

$$\int_\Omega \sigma(u) \cdot \nabla \eta^s dx = \int_\omega p_i \, \mathrm{div}(\eta) dx \ , \ \forall \eta \in \mathcal{V} \ . \tag{2.8}$$

Some terms in the above variational equation require explanation. The stress tensor $\sigma(\varphi)$ is given by

$$\sigma(\varphi) = \rho \mathbb{C} \nabla \varphi^s \ , \tag{2.9}$$

where the parameter ρ is given by (2.1). We consider isotropic material, so that the elasticity tensor $\mathbb{C}$ can be represented by the Lamé's coefficients μ and λ in the following form:

$$\mathbb{C} = 2\mu \mathbb{I} + \lambda (\mathrm{I} \otimes \mathrm{I}) \ , \tag{2.10}$$

where I and $\mathbb{I}$ are the second and fourth order identity tensors, respectively. The strain tensor $\nabla \varphi^s$ is given by the symmetric part of the gradient of φ, namely

$$\nabla \varphi^s = \frac{1}{2} (\nabla \varphi + (\nabla \varphi)^\top) \ . \tag{2.11}$$

The set $\mathcal{U}$ and the space $\mathcal{V}$ are defined as:

$$\mathcal{V} := \mathcal{U} := H_0^1(\Omega) \ . \tag{2.12}$$

The strong formulation associated to the variational problem (2.8) is given by: Find u, such that

$$\left\{ \begin{array}{rcll} \mathrm{div}\sigma(u) & = & 0 & \text{in} \quad \Omega \ , \\ \sigma(u) & = & \rho \mathbb{C} \nabla u^s, & \\ u & = & 0 & \text{on} \quad \partial\Omega \ , \\ [\![u]\!] & = & 0 \\ [\![\sigma(u)]\!] \, n & = & -p_i n \end{array} \right\} \text{on} \quad \partial\omega \ , \tag{2.13}$$

where the operator $[\![\varphi]\!]$ is used to denote the jump of the function φ on the interface $\partial\omega$, namely $[\![\varphi]\!] = \varphi_{|\Omega \setminus \overline{\omega}} - \varphi_{|\omega}$ on $\partial\omega$. The transmission condition on the interface $\partial\omega$ comes out from the variational formulation (2.8).

As can be seen, the hydraulic fracture model is a simple extension of the Francfort-Marigo damage model. Thus, the damage evolution is based just on the energy density distribution. One well-known limitation is that this kind of models are not able to distinguish between traction and compression stress states, so that some phenomena, such as crack closure or lips interpenetration for example, cannot be captured. However, the mechanism of hydraulic fracturing is such that these drawbacks do not apply, being the crack opening purely of traction-type, i.e., the crack faces are forced to move away.

2.3. **Statement of the optimization problem.** The minimization problem we are dealing with can be defined in the following way: for each time increment t_i,

$$\underset{\omega \subset \Omega}{\mathrm{Minimize}} \ \mathcal{F}_\omega(u) \ , \ \text{subject to (2.8)} \ , \tag{2.14}$$

where $\mathcal{F}_\omega(u)$ is given by (2.6).

A natural approach to deal with such a minimization problem consists in appealing to the topological derivative concept. The basic idea consists in evaluating the topological derivative of the shape functional (2.6) with respect to the nucleation of a small circular pressurized inclusion. Then, the associated topological derivative can be used as a descent direction to solve the minimization problem (2.14) indicating, at each iteration, the regions that have to be damaged.

In the context of hydraulic fracture, the fault-activation pressure is the specific value of the pressure at which activation of the geological fault takes place. An important feature

associated to the proposed hydraulic fracture model concerns the characterization of such a critical pressure. The difficulty to deal with problems with stress singularities by using Francfort-Marigo model is that the strain energy density rises locally to unbounded values at the crack tip and consequently above any finite threshold. Nevertheless, experiments like those of Griffith indicate the existence of a critical nonzero load even in the presence of such singularities, which reveals a limitation on the straightforward application of the Francfort-Marigo model in these cases. Note that in the case of damage this singularity is not observed. As a matter of fact, the same difficulty is observed to characterize the critical pressure in the context of hydraulic fracture phenomenon. In this sense, it is necessary to verify by some numerical strategy if the hydraulic fracture model permits the characterization of such a critical pressure. There exists some remedies available in the literature to bypass this problem, see for instance Allaire et al. (2011). We are adopting here the same strategy proposed by Xavier et al. (2017). The idea consists in introducing a new material property κ_s used together with a scaling factor given by the width δ of the initial damage. In particular, we replace κ by a modified energy release parameter κ_δ defined as

$$\kappa = \kappa_\delta := \frac{\kappa_s}{\delta} \, . \tag{2.15}$$

From the physical point of view, when δ becomes smaller, the parameter κ_δ increases in a similar way as the energy density, so that the critical pressure converges to a finite nonzero value. This strategy has shown to be effective in problems of crack propagation where the fracture is represented by a damaged region of small width δ, since letting $\delta \to 0$ forces the damaged region to be crack-like.

3. Topological derivative

The topological sensitivity analysis provides a scalar field, called topological derivative (Sokołowski and Żochowski, 1999), that represents the first order correction of the topological asymptotic expansion of a given shape functional with respect to the introduction of infinitesimal perturbations such as holes, inclusions, source terms or cracks. In other words, the topological derivative measures the sensitivity of the shape functional with respect to the introduction of topological perturbation. The topological derivative of the shape functional (2.6), with respect to the nucleation of a ball-shaped pressurized inclusion, is given by the sum (Novotny and Sokołowski, 2013)

$$D_T\mathcal{F}_\omega(x) = D_T\mathcal{J}(x) + \kappa_\delta D_T|\omega|(x) \quad \forall x \in \Omega \, , \tag{3.1}$$

where the topological derivative of the Griffith type dissipation energy term, $\kappa_\delta D_T|\omega|(x)$, is trivially obtained and given by

$$\kappa_\delta D_T|\omega|(x) = \begin{cases} +\kappa_\delta, & \text{if } \; x \in \Omega \setminus \overline{\omega} \, , \\ -\kappa_\delta, & \text{if } \; x \in \omega \, . \end{cases} \tag{3.2}$$

On the other hand, the topological derivative of the total potential energy of the system, $D_T\mathcal{J}(x)$, can be obtained as a particular case with respect to the one treated by Xavier and Novotny (2017). However, for the sake of completeness, the derivations associated to our model problem is shown in Appendix A. Since we are using a very weak material to replace the damaged pressurized region, we can take the limit cases $\gamma \to 0$ and $\gamma \to \infty$ in (A.46). Formally, for $\gamma \to 0$ the inclusion represents a hole and the transmission condition on the boundary of the inclusion degenerates itself to a non-homogeneous Neumann boundary condition. In this case the topological derivative evaluated within the elastic material $\Omega \setminus \overline{\omega}$ becomes

$$D_T\mathcal{F}_\omega(x) = -\mathbb{P}_0\sigma(u)(x) \cdot \nabla u^s(x) - (1+\alpha)\, p_i \, \mathrm{div}(u)(x) - \frac{p_i^2}{2\mu} + \kappa_\delta \, , \quad \forall x \in \Omega \setminus \overline{\omega} \, , \tag{3.3}$$

with the polarization tensor $\mathbb{P}_0$ given by

$$\mathbb{P}_0 = \frac{2\mu+\lambda}{\mu+\lambda}\left(\mathbb{I} - \frac{\mu-\lambda}{4\mu}\mathrm{I}\otimes\mathrm{I}\right) . \tag{3.4}$$

In addition, when $\gamma \to \infty$, the topological perturbation represents a rigid inclusion. In this case the topological derivative evaluated into the compliant material ω results in

$$D_T\mathcal{F}_\omega(x) = -\mathbb{P}_\infty\sigma(u)(x)\cdot\nabla u^s(x) - \kappa_\delta , \quad \forall x \in \omega , \tag{3.5}$$

where the polarization tensor $\mathbb{P}_\infty$ is given by

$$\mathbb{P}_\infty = -\frac{2\mu+\lambda}{3\mu+\lambda}\left(\mathbb{I} + \frac{\mu-\lambda}{4(\mu+\lambda)}\mathrm{I}\otimes\mathrm{I}\right) . \tag{3.6}$$

Remark 1. *It should be noted that, according to Giusti et al. (2016), the same formula* (3.1) *holds true for heterogeneous medium, provided that the heterogeneity is locally Lipschitz continuous.*

4. Topology optimization algorithm

In this section the obtained topological derivative expression is used to devise a simple topology optimization algorithm specifically designed to simulate the whole nucleation and propagation process of hydraulic fracturing. This algorithm was originally proposed by Xavier et al. (2017). It is based on the fact that the introduction of an infinitesimal inclusion at the region where the topological derivative is negative allow for a decreasing on the values of the shape functional. For the sake of completeness, in this section the adapted version of the algorithm to the context of hydraulic fracturing process is presented. For more details see Xavier et al. (2017).

The present algorithm is based on the introduction of a pressurized inclusion at the region where the topological derivative is negative. If the size of the inclusion is small enough to corroborate with the theory, but at the same time large enough to be treated numerically, it is expected that the shape functional (2.6) decreases. The size of inclusion is associated with the region ω^* where the topological derivative field is negative, i.e.,

$$\omega^* := \{x \in \Omega : D_T\mathcal{F}_\omega(x) < 0\} . \tag{4.1}$$

In principle ω^* must not be a connected subset, that is, there might be nucleation of damage in front of the previously damaged zone, but also elsewhere in the body. In the first case, nucleation of damage yields evolution of the damage set, whereas in the latter it means genuine damage nucleation. Let us emphasize that from a theoretical point of view, the topological derivative holds away from the damaged region and for an infinitesimal inclusion only. On the other hand, the topological derivative is defined through a limit passage when the small parameter governing the size of the topological perturbation goes to zero, so that it can be used as a steepest-descent direction in an optimization process like in any method based on the gradient of the objective functional. Therefore, for practical purposes, since the numerical method introduces a grid of finite size, we will consider nucleation of inclusions of finite sizes but small enough such that a decreasing of the proposed functional in each iteration is ensured.

The algorithm can be designed either by nucleating only at those points where the topological derivative achieves its minimum, or at all points were it is negative. On the other hand, an intermediate choice would be to calibrate the size of the inclusion to be nucleated according to the characteristic size of the previously damaged region. This choice will be provided by the model parameter $\beta \in (0, 1)$, with the extreme choices given

by $\beta = 0$ (minimum points only), and $\beta = 1$ (the whole negative region), respectively. To this aim, let us introduce the quantity

$$D_T\mathcal{F}^*_\omega := \min_{x\in\omega^*} D_T\mathcal{F}_\omega(x) \ , \tag{4.2}$$

which allows us to define the inclusion to be nucleated $\omega^\beta \subset \omega^*$ as follows

$$\omega^\beta := \{x \in \omega^* : D_T\mathcal{F}_\omega(x) \leq (1-\beta)D_T\mathcal{F}^*_\omega\} \ , \tag{4.3}$$

where $\beta \in (0, 1)$ is chosen such that $|\omega^\beta| \approx (\pi l^2)/4$ (with $l \leq \delta$), so that the size of the inclusion to be nucleated is here related to the width δ of the initial damage. Therefore, if the initial damage is crack-like (δ small), β will be taken as small as to satisfy $|\omega^\beta| \leq (\pi l^2)/4$. By this choice, a damage will evolve like a crack. As a matter of fact, the parameter β induces a threshold for the topological derivative $D_T\mathcal{F}_\omega(x)$ and the volume of the inclusion will only depend on l, while its shape and location will depend on the contour lines (level-sets) of $D_T\mathcal{F}_\omega$. We will show through some numerical experiments that this strategy ensures a decreasing of the proposed functional at each iteration, provided that the size of the inclusion to be nucleated ω^β is small enough.

The algorithm can be outlined as follows. Given the solution of the linear elasticity system (2.8), the associated topological derivative field (3.1) is evaluated. If the field is positive everywhere or $|\omega^*| < (\pi l^2)/4$, a perturbation of size $(\pi l^2)/4$ at any point of the domain is likely to increase the value of the functional. In this case, the algorithm will not propagate the damage, and it is possible to increase the pressure p_i further and run a new analysis. On the contrary, if the topological derivative field is negative in some undamaged region and the condition $|\omega^*| \geq (\pi l^2)/4$ is fulfilled, a damage ω^β will be nucleated inside ω^*, with $\beta : |\omega^\beta| \approx (\pi l^2)/4$. Schematically, one can see the newly-damaged region as an half-disk of radius $l/2$ located at the tip of the pre-existing damage. Since the nucleation of a new damage ω^β modifies the problem, the solution to the elasticity system associated with the new topology need to be computed again. Finally, the new topological derivative field is evaluated and the process is repeated until the condition $|\omega^*| \geq (\pi l^2)/4$ is no more fulfilled for any pressure increment. The elasticity system is solved by the finite element method. In order to improve the numerical results, the mesh at the crack tip is intensified in each iteration of the optimization process. As presented by Xavier et al. (2017), the above procedure can also be written in the form of pseudo-code, see Algorithm 1.

5. Numerical experiments

As mentioned in Section 1, the reference domain Ω stands for one block of the idealized reservoir, i.e., a limited region which contains an initial damage representing a single geological fault, see Figure 1. The topology is identified by the elastic material distribution and the compliant material is used to represent the geological fault. We assume that in all examples the structure is under plane strain assumption and that the total intensity of the pressure p was divided into N uniform increments. In addition, the elasticity problem is discretized by using linear triangular elements only.

5.1. **Elementary example.** In this first example, the hold-all domain Ω is given by a square with dimension $(5 \times 5)m^2$ as shown in Figure 3. Homogeneous Dirichlet boundary conditions are considered in all sides of the domain. A pre-existing geological fault, represented by the initial damage of length h and width δ, is located at the center of the bottom side immediately above the pressurization well. The material properties such as the modulus of elasticity E and the Poisson ratio ν correspond to the values used by Pereira et al. (2014). In addition, the inclusion is made of a material with an elasticity modulus $\rho_0 E$ and its diameter is specified by the parameter l. The total intensity of the

Algorithm 1: The damage evolution algorithm.

input : Ω, ω, l, N, p_0, Δp_i
output: The optimal topology $\omega^\star$

```
for i = 1 : N do
    solve elasticity system (2.8);
    evaluate the topological derivative D_T F_ω according to (3.1);
    compute the threshold ω* from (4.1);
    while |ω*| ≥ (πl²)/4 do
        intensify the mesh at the crack tip;
        solve elasticity system and evaluate D_T F_ω;
        compute the threshold ω* from (4.1);
        compute the threshold ω^β from (4.3);
        nucleated new inclusion ω^β inside ω*;
        update the damaged region: ω ← ω ∪ ω^β;
        solve elasticity system and evaluate D_T F_ω;
        compute the threshold ω* from (4.1);
    end while
end for
```

pressure is $p = 8$ MPa and was divided into $N = 200$ uniform increments. All these data are summarized in Table 1.

TABLE 1. Elementary example: Parameters.

Parameter	Value	Parameter	Value
h	1,0 m	E	30 GPa
δ	0,025 m	ρ_0	10^{-6}
l	$(2/3)\delta$	ν	0,3
p	8 MPa	κ_s	320,0 J/m

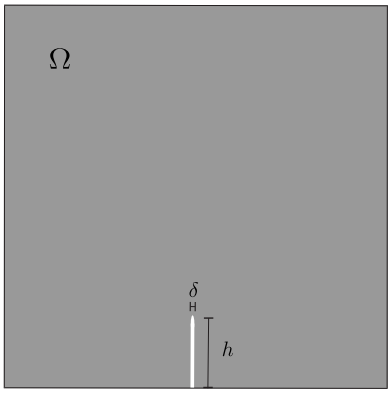

FIGURE 3. Elementary example: Geometry.

5.1.1. *Critical pressure.* As mentioned in Section 2, it is necessary to verify whether the proposed hydraulic fracture model permits the characterization of the fault-activation pressure. To this aim, five tests were made with different values for the initial width δ of the damage, namely $\delta \in \{\frac{1}{20}, \frac{1}{40}, \frac{1}{80}, \frac{1}{160}, \frac{1}{320}\}$[m]. The parameters were maintained

according to Table 1. The critical pressure p_c was selected as the value of the current pressure which allows the nucleation of the first inclusion, that is, when the condition $|\omega^*| \geq (\pi l^2)/4$ holds for the first time. Figure 4 illustrates the critical pressure obtained for the different tests, which are normalized according to the first estimate found for the critical pressure p_c^0. Therefore, the introduction of the parameter κ_δ through (2.15) allows for dealing with a feasible critical pressure as shown in Figure 4 (blue bullet line). We claim however that it is an *ad hoc* correction of the model which works for $\delta > 0$. The limiting case $\delta \to 0$ is much more involved and has been partially addressed by Van Goethem and Novotny (2010), for instance. However, the proper variational limit is currently out of reach for the planar vectorial problem (i.e., without the anti-plane assumption). As

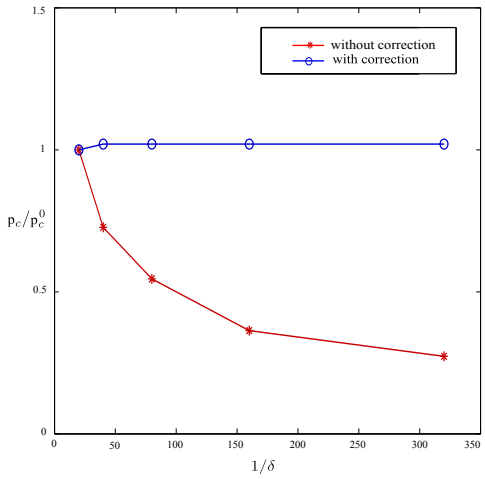

FIGURE 4. Elementary example: Convergence analysis for the critical pressure.

expected, with the decrease of the width δ, the energy density at the crack tip increases. Note that without a scale factor correction, the critical pressure decreases towards zero. On the other hand, the use of the factor δ leads to an asymptotic behavior for the critical pressure.

Remark 2. *The result shown in Figure 4 can be seen as a numerical evidence of the mathematical convergence of the proposed approach to a hydraulic fracture model in its strict sense. Therefore, the study of such underlying mathematical convergence is an important topic which will be treated in future works.*

5.1.2. *Damage evolution.* The damage distribution at iteration number 215 is shown in Figure 5(a). Note that the crack trajectory occurs in a straight line as expected. The pressure has been incremented 80 times to comply with the propagation criterion. Moreover, the observed critical pressure is $p_c = 3.2$ MPa. Note that the model dissipates energy at each iterations, as shown in Figure 5(b).

5.2. **Transverse wells.** This second example has the same geometry and boundary conditions of the previous one. However, in the present case two transverse wells centered at the points $c_1 = (2.8, 1.5)$ and $c_2 = (2.8, 2.5)$ and with diameters $d_1 = 0.3\ m$ and $d_2 = 0.7\ m$, respectively, are considered. See Figures 6(a) and 7(a). In this example, the total intensity of the pressure is $p = 6$ MPa and was divided into $N = 150$ uniform increments. The remainder parameters being chosen according to Table 1. In addition, two different situations are considered. The first one (case 1) considers that the transverse wells are not pressurized. In the second situation (case 2) the transverse wells are pressurized and the intensity of the pressure is the same as that inside the initial damage. Thus, the scope of this study is the influence of these transverse wells on the crack trajectory.

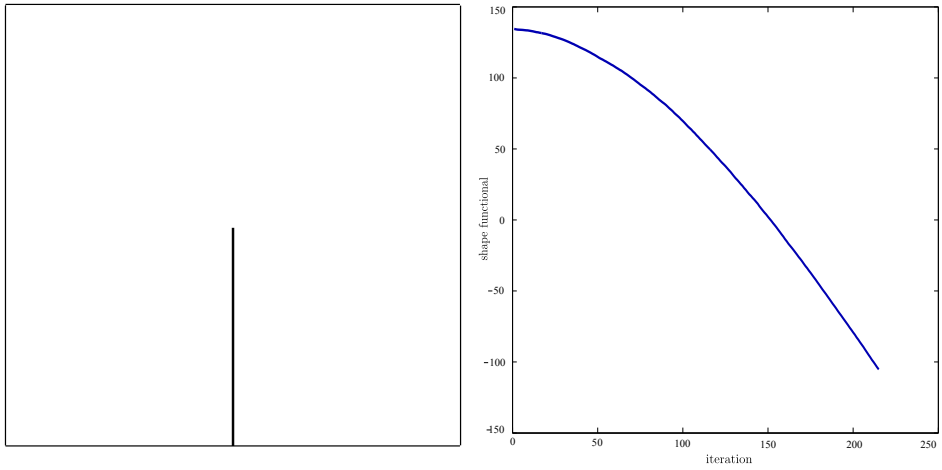

(a) Final result (b) Total energy $\mathcal{F}_\omega(u)$ from (2.6)

FIGURE 5. Elementary example.

The final results are shown in Figures 6(b) and 7(b). In the case 1 the observed critical pressure is $p_c = 3.24$ MPa. Note that in this case the smaller *no-pressurized* transverse well only affect the crack trajectory. After then, the crack tip attains the second transverse well. In the case 2, the observed critical pressure is $p_c = 3.2$ MPa. In this case, the smaller *pressurized* transverse well attracts abruptly the crack trajectory. After then, the crack tip attains the second transverse well again. In addition, it can be verified from the case 2 that the proposed algorithm was able to activate the mechanism of damage nucleation, independently of any initial damaged region on the boundary of the smaller transverse well. As matter of fact, the critical pressure associated to the nucleation phenomenon was $p_c = 4.08$ MPa. Finally, the behavior of the square root of the strain energy, defined by

$$\mathcal{E}(u) = \sqrt{\frac{1}{2}\int_\Omega \sigma(u) \cdot \nabla u^s}\ , \tag{5.1}$$

in both cases, is shown in Figure 8.

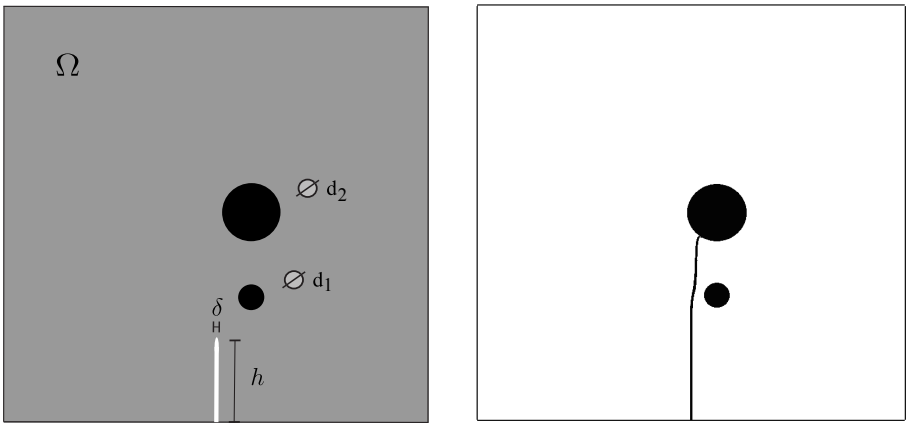

(a) geometry (b) final result

FIGURE 6. Case 1: No-pressurized transverse wells.

This example suggests a potential strategy to control the crack trajectories by inserting transverse wells into the reservoir. However, it should be emphasized that, due to the

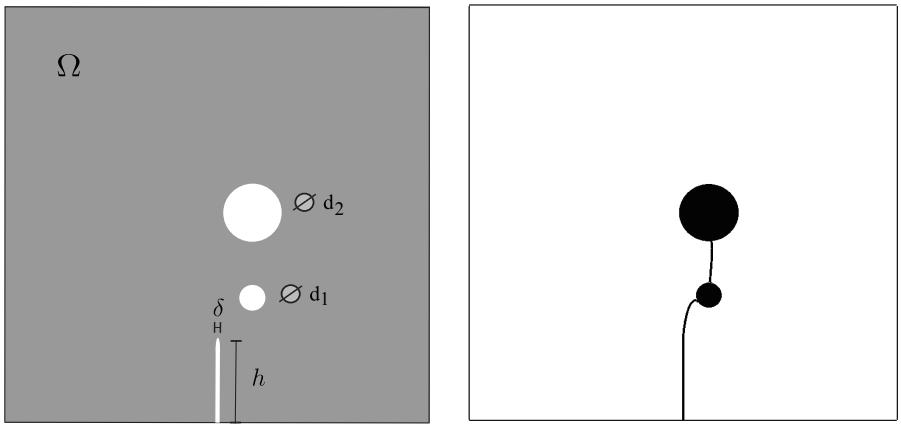

(a) geometry (b) final result

FIGURE 7. Case 2: Pressurized transverse wells.

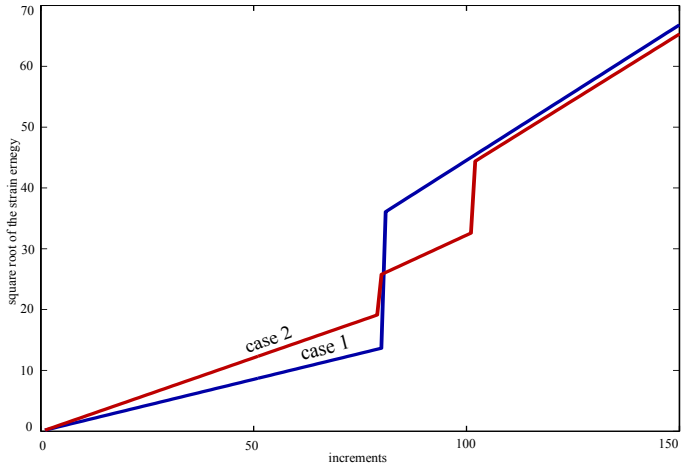

FIGURE 8. Transverse wells: Square root of the strain energy $\mathcal{E}(u)$ from (5.1).

many simplifications here adopted, the obtained results are purely academic and should not be interpreted as a prediction associated to the real-life case.

5.3. **Stratified block.** In this example, we consider an heterogeneous material: the block is composed by two layers with different elasticity modulus, namely, $E_1 = 30$ GPa and $E_2 = 60$ GPa. In addition, the geometry and boundary conditions are the same as proposed in the elementary example of Section 5.1. The different cases treated in this example differ from each other by the spatial distribution of the material properties E_1 and E_2, as shown in Figures 9(a) and 10(a). The remainder parameters being chosen according to Table 1.

The damage distributions at iteration number 215 are shown in Figures 9(b) and 10(b). In the first case, the observed critical pressure is $p_c = 3.32$ MPa. Note that in this scenario, the trajectory of the fracture follows the direction of the interface between the two materials when the crack tip attains the stiffer layer. In the second case, the observed critical pressure is $p_c = 4.4$ MPa. In this situation the trajectory of the fracture only suffers a little change in its direction when the crack tip attains the weaker layer.

5.4. **Heterogeneous medium.** In this last example a heterogeneous medium is considered. The geometry, boundary conditions and the parameters are the same of the

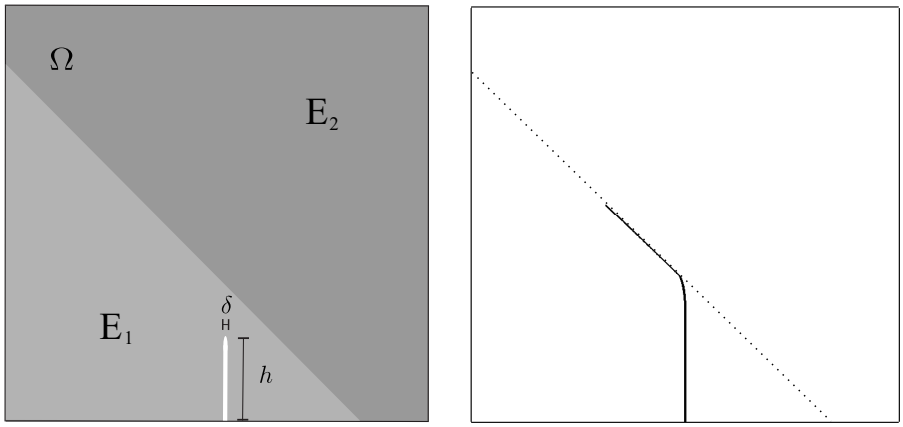

(a) geometry (b) final result

FIGURE 9. Stratified block: Case 1.

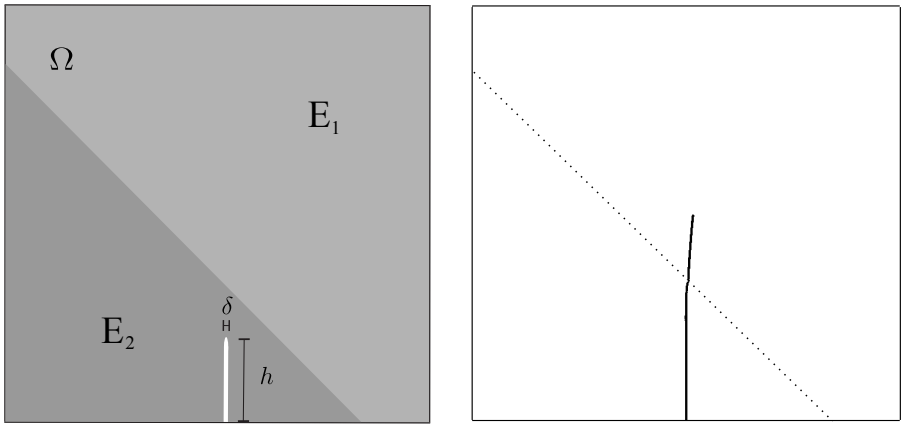

(a) geometry (b) final result

FIGURE 10. Stratified block: Case 2.

elementary example of Section 5.1. However, in this case the Young modulus E is corrupt with White Gaussian Noise (WGN) of zero mean and standard deviation τ. Therefore, E is replaced by $E_\tau = E(1 + s\tau)$, where $s : \Omega \to \mathbb{R}$ is a function assuming random values in the interval $(0, 1)$ and $\tau = 5$ corresponds to the noise level. The Figures 11(a) and 11(b) shows the corrupted Young modulus $E_\tau(x)$ and the damage distribution at iteration number 347, respectively. The observed critical pressure is $p = 7.92$ MPa. Note that, due to the medium heterogeneity, we can observe kinking and bifurcations phenomena, which is in agreement with what it is expected from the physical point of view.

6. Concluding remarks

This paper has demonstrated that the linear and variational fracture model introduced by Francfort and Marigo may be applied to hydraulic fracturing process, by means of an original use of topological derivative concept. In particular, a simplified hydraulic fracture model obtained by adapting the one introduced by Francfort and Marigo to the context of hydraulic fracturing process has been proposed. A shape functional given by the sum of the total potential energy of the system with a Griffith-type dissipation energy term has been minimized with respect to a set of ball-shaped pressurized inclusions by using

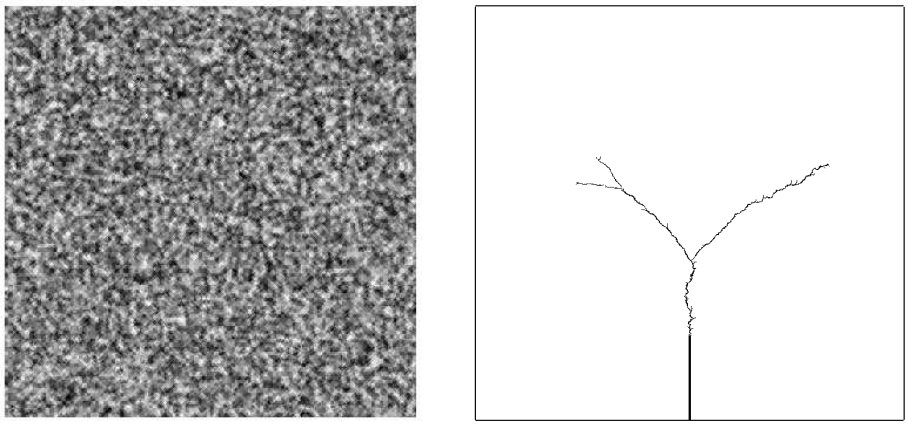

(a) corrupted Young modulus (b) final result

FIGURE 11. Heterogeneous medium.

the topological derivative concept. In particular, the topological asymptotic expansion of such shape functional, with respect to the nucleation of a circular inclusion endowed with non-homogeneous transmission condition on its boundary, has been obtained. In addition, we have shown that the associated topological derivative corroborates with the famous Eshelby theorem. The obtained result has been used to devise a topology optimization algorithm specifically designed to simulate the whole nucleation and propagation process of hydraulic fracturing. The strikingly simplicity of the proposed topological derivative-based fracking modelling should be noted. In fact, since the loading, given by the prescribed pressure acting within the damaged region, comes out naturally from the variational formulation, just a minimal number of user-defined algorithmic parameters is required. Finally, we have presented four test cases showing typical features of hydraulic fracturing process, including the characterization of the fault-activation pressure as well as specific crack path growth, allowing for kinking and bifurcations. Further studies related to the underlying mathematical convergence of the model, introduction of body forces, fluid-structure interaction as well as the three spatial dimensions case are required.

ACKNOWLEDGEMENTS

This research was partly supported by CNPq (Brazilian Research Council), CAPES (Brazilian Higher Education Staff Training Agency), ANP (National Agency of Petroleum, Natural Gas and Biofuels) and FAPERJ (Research Foundation of the State of Rio de Janeiro). These supports are gratefully acknowledged. Second author was supported by the FCT Starting Grant " Mathematical theory of dislocations: geometry, analysis, and modelling" (IF/00734/2013).

APPENDIX A. TOPOLOGICAL SENSITIVITY ANALYSIS

Let us consider an open and bounded domain $\Omega \subset \mathbb{R}^2$ with a Lipschitz boundary $\partial\Omega$, which is subject to a nonsmooth perturbation confined in a small region $B_\varepsilon(\hat{x})$ of size ε centered at an arbitrary point $\hat{x} \in \Omega$, as sketched in Figure 12. We introduce a characteristic function $x \mapsto \chi(x)$, $x \in \mathbb{R}^2$, associated with the unperturbed domain, namely $\chi = \mathbb{1}_\Omega$, such that:

$$|\Omega| = \int_{\mathbb{R}^2} \chi(x) dx \,, \tag{A.1}$$

where $|\Omega|$ is the Lebesgue's measure of Ω. Then, we define a characteristic function associated with the topologically perturbed domain of the form $x \mapsto \chi_\varepsilon(\hat{x}; x)$, $x \in \mathbb{R}^2$. In the case of a perforation, for example, $\chi_\varepsilon(\hat{x}) = \mathbb{1}_\Omega - \mathbb{1}_{B_\varepsilon(\hat{x})}$, the perforated domain is obtained as $\Omega_\varepsilon(\hat{x}) = \Omega \setminus \overline{B_\varepsilon(\hat{x})}$. Then, we assume that a given shape functional $\psi(\chi_\varepsilon(\hat{x}))$, associated with the topologically perturbed domain, admits the following topological asymptotic expansion:

$$\psi(\chi_\varepsilon(\hat{x})) = \psi(\chi) + f(\varepsilon) D_T\psi(\hat{x}) + o(f(\varepsilon)) \,, \tag{A.2}$$

where $\psi(\chi)$ is the shape functional associated to the original domain, that is, without perturbation, $f(\varepsilon)$ is a positive function such that $f(\varepsilon) \to 0$ when $\varepsilon \to 0$ and $o(f(\varepsilon))$ is the remainder. The function $\hat{x} \mapsto D_T\psi(\hat{x})$ is called the topological derivative of ψ at $\hat{x}$. Therefore, this derivative can be seen as a first order correction of $\psi(\chi_\varepsilon(\hat{x}))$. In fact, after rearranging (A.2) we have

$$\frac{\psi(\chi_\varepsilon(\hat{x})) - \psi(\chi)}{f(\varepsilon)} = D_T\psi(\hat{x}) + \frac{o(f(\varepsilon))}{f(\varepsilon)} \,. \tag{A.3}$$

The limit $\varepsilon \to 0$ in the above expression leads to the general definition for the topological derivative, namely

$$D_T\psi(\hat{x}) = \lim_{\varepsilon \to 0} \frac{\psi(\chi_\varepsilon(\hat{x})) - \psi(\chi(x))}{f(\varepsilon)} \,. \tag{A.4}$$

It is worth to mention that the topological derivative is defined by a limit passage when the small parameter governing the size of the topological perturbation goes to zero in (A.4). However, it can also be used as a steepest-descent direction in an optimization process like in any method based on the gradient of the cost functional.

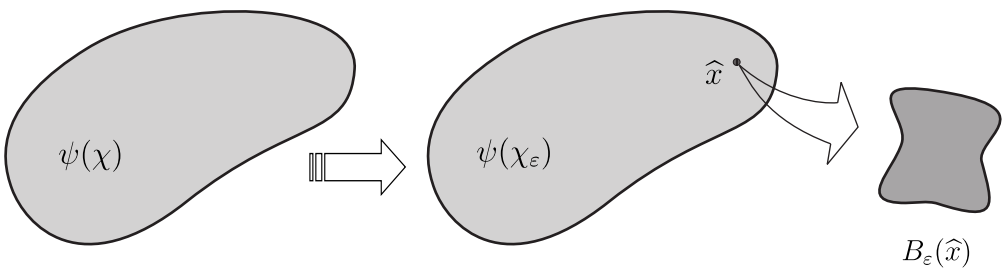

FIGURE 12. The topological derivative concept.

A.1. **Perturbed problem.** Let us introduce the topologically perturbed problem associated to the hydraulic fracture model. The idea consists in nucleating a circular inclusion, denoted by $B_\varepsilon(\hat{x})$, of radius ε and center at the arbitrary point $\hat{x} \in \Omega$, such that $\overline{B_\varepsilon(\hat{x})} \subset \Omega$ and $\overline{B_\varepsilon(\hat{x})} \cap \partial\omega = \varnothing$. We assume that $B_\varepsilon(\hat{x})$ is submitted to a pressure load, which leads to a non-homogeneous transmission condition on the interface $\partial B_\varepsilon(\hat{x})$. See sketch in Figure 13. In this case $\chi_\varepsilon(\hat{x})$ is defined as follows:

$$\chi_\varepsilon(\hat{x}) = \mathbb{1}_\Omega - (1-\gamma)\mathbb{1}_{B_\varepsilon(\hat{x})} \,, \tag{A.5}$$

where $\gamma = \gamma(x)$ is the contrast in the material properties. From these elements, we define a piecewise constant function of the form

$$\gamma_\varepsilon = \gamma_\varepsilon(x) := \begin{cases} 1 & \text{if } x \in \Omega \setminus \overline{B_\varepsilon} \,, \\ \gamma & \text{if } x \in B_\varepsilon \,. \end{cases} \tag{A.6}$$

The shape functional associated with the topologically perturbed problem is given by

$$\mathcal{F}_{\omega_\varepsilon}(u_\varepsilon) = \mathcal{J}_{\chi_\varepsilon}(u_\varepsilon) + \kappa|\omega_\varepsilon| \,, \tag{A.7}$$

where $\omega_\varepsilon = \omega \cup B_\varepsilon$ with $\omega \cap B_\varepsilon = \emptyset$. The total potential energy of the perturbed system, $\mathcal{J}_{\chi_\varepsilon}(u_\varepsilon)$, is given by

$$\mathcal{J}_{\chi_\varepsilon}(u_\varepsilon) = \frac{1}{2}\int_\Omega \sigma_\varepsilon(u_\varepsilon)\cdot\nabla u_\varepsilon^s dx - \int_\omega p_i \,\mathrm{div}(u_\varepsilon)dx - \int_{B_\varepsilon} p_i \,\mathrm{div}(u_\varepsilon)dx\ , \tag{A.8}$$

with the vector function u_ε solution of the following variational problem: Find $u_\varepsilon \in \mathcal{U}$, such that

$$\int_\Omega \sigma_\varepsilon(u_\varepsilon)\cdot\nabla\eta^s dx = \int_\omega p_i \,\mathrm{div}(\eta)dx + \int_{B_\varepsilon} p_i \mathrm{div}(\eta)dx\ ,\ \forall \eta \in \mathcal{V}, \tag{A.9}$$

where the Cauchy stress tensor $\sigma_\varepsilon(u_\varepsilon) = \gamma_\varepsilon\sigma(u_\varepsilon)$ with γ_ε given by (A.6).

The strong formulation associated with the variational problem (A.9) is given by: Find u_ε, such that:

$$\left\{\begin{array}{rcll} \mathrm{div}\sigma_\varepsilon(u_\varepsilon) &=& 0 & \text{in}\quad \Omega\ , \\ \sigma_\varepsilon(u_\varepsilon) &=& \gamma_\varepsilon\sigma(u_\varepsilon)\ , & \\ u_\varepsilon &=& 0 & \text{on}\quad \partial\Omega\ , \\ \left.\begin{array}{r}[\![u_\varepsilon]\!] \\ [\![\sigma_\varepsilon(u_\varepsilon)]\!]\, n\end{array}\right. &=& \left.\begin{array}{l} 0 \\ -p_i n\end{array}\right\} & \text{on}\quad \partial\omega\ , \\ \left.\begin{array}{r}[\![u_\varepsilon]\!] \\ [\![\sigma_\varepsilon(u_\varepsilon)]\!]\, n\end{array}\right. &=& \left.\begin{array}{l} 0 \\ -p_i n\end{array}\right\} & \text{on}\quad \partial B_\varepsilon\ . \end{array}\right. \tag{A.10}$$

Again, the transmission conditions on the interfaces $\partial\omega$ and ∂B_ε stem from the variational formulation (A.9).

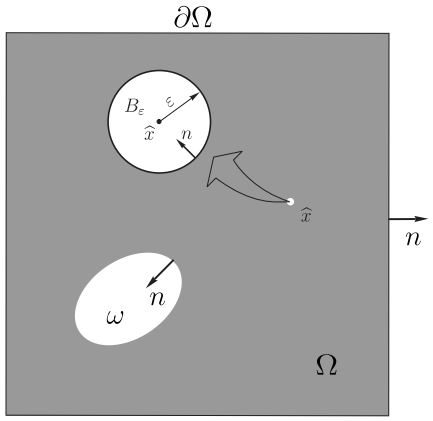

FIGURE 13. Perturbed problem.

A.2. **The existence of the associated topological derivative.** The existence of the associated topological derivative is ensured by the following result:

Lemma 3. *Let u_ε and u be solutions of problems* (A.9) *and* (2.8)*, respectively. Then, the following estimate holds true:*

$$\|u_\varepsilon - u\|_{H^1(\Omega)} \leq C\varepsilon\ , \tag{A.11}$$

where C is a constant independent of the small parameter ε.

Proof. Let us subtract (2.8) from (A.9). Then, from the definition for the contrast (A.6), we obtain

$$\begin{aligned}\int_{B_\varepsilon} p_i \,\mathrm{div}(\eta)dx &= \int_\Omega (\sigma_\varepsilon(u_\varepsilon) - \sigma(u))\cdot\nabla\eta^s dx \\ &= \int_{\Omega\setminus B_\varepsilon} (\sigma(u_\varepsilon) - \sigma(u))\cdot\nabla\eta^s dx + \int_{B_\varepsilon} (\gamma\sigma(u_\varepsilon) - \sigma(u))\cdot\nabla\eta^s dx\ .\end{aligned}$$

After adding and subtracting the term

$$\int_{B_\varepsilon} \gamma\sigma(u)\cdot\nabla\eta^s dx$$

in the above expression we have:

$$\int_{B_\varepsilon} p_i\,\mathrm{div}(\eta)dx = \int_\Omega \sigma_\varepsilon(u_\varepsilon-u)\cdot\nabla\eta^s dx + \int_{B_\varepsilon}(\gamma-1)\sigma(u)\cdot\nabla\eta^s dx\,. \tag{A.12}$$

By taking $\eta = u_\varepsilon - u$ as test function in (A.12) we obtain the following equality:

$$\int_\Omega \sigma_\varepsilon(u_\varepsilon-u)\cdot\nabla(u_\varepsilon-u)^s dx = \int_{B_\varepsilon}(1-\gamma)\sigma(u)\cdot\nabla(u_\varepsilon-u)^s dx + \int_{B_\varepsilon} p_i\,\mathrm{div}(u_\varepsilon-u)dx\,.$$

From the above expression, we have

$$\int_\Omega \sigma_\varepsilon(u_\varepsilon-u)\cdot\nabla(u_\varepsilon-u)^s dx = \int_{B_\varepsilon}\mathrm{T}(u)\cdot\nabla(u_\varepsilon-u)^s dx\,, \tag{A.13}$$

where we have introduced the notation

$$\mathrm{T}(u) = (1-\gamma)\sigma(u) + p_i\mathrm{I}\,. \tag{A.14}$$

From Cauchy-Schwartz inequality it follows that

$$\begin{aligned}\int_\Omega \sigma_\varepsilon(u_\varepsilon-u)\cdot\nabla(u_\varepsilon-u)^s dx &\le \|\mathrm{T}(u)\|_{L^2(B_\varepsilon)}\|\nabla(u_\varepsilon-u)\|_{L^2(B_\varepsilon)}\\ &\le c_0\varepsilon\|\nabla(u_\varepsilon-u)\|_{L^2(B_\varepsilon)}\\ &\le c_1\varepsilon\|u_\varepsilon-u\|_{H^1(\Omega)}\,.\end{aligned} \tag{A.15}$$

From the coercivity of the bilinear form on the left-hand side of (A.15) we have

$$c\|u_\varepsilon-u\|^2_{H^1(\Omega)} \le \int_\Omega \sigma_\varepsilon(u_\varepsilon-u)\cdot\nabla(u_\varepsilon-u)^s dx\,, \tag{A.16}$$

which leads to the result with $C = c_1/c$ independent of the small parameter ε. □

A.3. **Topological derivative evaluation.** In order to evaluate the difference between the functionals $\mathcal{J}(u)$ and $\mathcal{J}_{\chi_\varepsilon}(u_\varepsilon)$, respectively defined in (2.7) and (A.8), we start by taking $\eta = u_\varepsilon - u$ as test function in the variational problem (2.8). Then we have the following equality

$$\int_\Omega \sigma(u)\cdot\nabla u^s dx = \int_\Omega \sigma(u)\cdot\nabla u_\varepsilon^s dx - \int_\omega p_i\,\mathrm{div}(u_\varepsilon-u)dx\,. \tag{A.17}$$

After replacing (A.17) into (2.7) we obtain

$$\mathcal{J}(u) = \frac{1}{2}\int_\Omega \sigma(u)\cdot\nabla u_\varepsilon^s dx - \frac{1}{2}\int_\omega p_i\,\mathrm{div}(u_\varepsilon+u)dx\,. \tag{A.18}$$

In the same way, let us set $\eta = u_\varepsilon - u$ as test function in the variational problem (A.9). Thus

$$\begin{aligned}\int_\Omega \sigma_\varepsilon(u_\varepsilon)\cdot\nabla u_\varepsilon^s dx = \int_\Omega \sigma_\varepsilon(u_\varepsilon)\cdot\nabla u^s dx\\ + \int_\omega p_i\,\mathrm{div}(u_\varepsilon-u)dx + \int_{B_\varepsilon} p_i\,\mathrm{div}(u_\varepsilon-u)dx\,.\end{aligned} \tag{A.19}$$

After replacing (A.19) into (A.8), it follows

$$\mathcal{J}_{\chi_\varepsilon}(u_\varepsilon) = \frac{1}{2}\int_\Omega \sigma_\varepsilon(u_\varepsilon)\cdot\nabla u^s dx - \frac{1}{2}\int_\omega p_i\,\mathrm{div}(u_\varepsilon+u)dx - \frac{1}{2}\int_{B_\varepsilon} p_i\,\mathrm{div}(u_\varepsilon+u)dx\,. \tag{A.20}$$

From (A.18) and (A.20), the variation of the energy shape functionals can be written as

$$\mathcal{J}_{\chi_\varepsilon}(u_\varepsilon) - \mathcal{J}(u) = \frac{1}{2}\int_\Omega \sigma_\varepsilon(u_\varepsilon)\cdot\nabla u^s dx - \frac{1}{2}\int_\Omega \sigma(u_\varepsilon)\cdot\nabla u^s dx \\ - \frac{1}{2}\int_{B_\varepsilon} p_i \,\mathrm{div}(u_\varepsilon + u)dx\,. \quad \text{(A.21)}$$

Now, by taking into account the definition for the contrast γ_ε given by (A.6), we have

$$\mathcal{J}_{\chi_\varepsilon}(u_\varepsilon) - \mathcal{J}(u) = \frac{1}{2}\int_{\Omega\setminus B_\varepsilon} \sigma(u_\varepsilon)\cdot\nabla u^s dx + \frac{1}{2}\int_{B_\varepsilon} \gamma\sigma(u_\varepsilon)\cdot\nabla u^s dx \\ - \frac{1}{2}\int_{\Omega\setminus B_\varepsilon} \sigma(u_\varepsilon)\cdot\nabla u^s dx - \frac{1}{2}\int_{B_\varepsilon} \sigma(u_\varepsilon)\cdot\nabla u^s dx - \frac{1}{2}\int_{B_\varepsilon} p_i \,\mathrm{div}(u_\varepsilon + u)dx\,. \quad \text{(A.22)}$$

Let us add and subtract the term

$$\frac{1}{2}\int_{B_\varepsilon} p_i \,\mathrm{div}(u)dx\,. \quad \text{(A.23)}$$

Thus, the following expression is obtained after canceling the identical terms

$$\mathcal{J}_{\chi_\varepsilon}(u_\varepsilon) - \mathcal{J}(u) = \int_{B_\varepsilon} \frac{\gamma-1}{2\gamma}\sigma_\varepsilon(u_\varepsilon)\cdot\nabla u^s dx \\ - \int_{B_\varepsilon} p_i \,\mathrm{div}(u)dx - \frac{1}{2}\int_{B_\varepsilon} p_i \,\mathrm{div}(u_\varepsilon - u)dx\,. \quad \text{(A.24)}$$

Note that the variation of the energy shape functional results in an integral concentrated into the inclusion B_ε. Therefore, in order to apply the definition for the topological derivative given by (A.2), we need to know the asymptotic behavior of the function u_ε with respect the small parameter ε. Thus, let us introduce the following ansätz:

$$u_\varepsilon = u + w_\varepsilon + \tilde{u}_\varepsilon\,, \quad \text{(A.25)}$$

where u is solution of the unperturbed problem (2.13), w_ε is solution to an auxiliary exterior problem and $\tilde{u}_\varepsilon$ is the remainder.

In particular, the following auxiliary boundary value problem is considered and formally obtained when $\varepsilon \to 0$: Find $S_\varepsilon(w_\varepsilon)$, such that

$$\left\{\begin{array}{rcll} \mathrm{div} S_\varepsilon(w_\varepsilon) &=& 0 & \text{in } \mathbb{R}^2\,, \\ S_\varepsilon(w_\varepsilon) &\to& 0 & \text{in } \infty\,, \\ [\![S_\varepsilon(w_\varepsilon)]\!]\, n &=& g & \text{on } \partial B_\varepsilon\,, \end{array}\right. \quad \text{(A.26)}$$

where $S_\varepsilon(w_\varepsilon) = \gamma_\varepsilon \mathbb{C}\nabla w_\varepsilon^s$ and $g = ((\gamma-1)S(u)(\hat{x}) - \rho^{-1}p_i\mathrm{I})n$ has been obtained from a Taylor series expansion of $\sigma(u(x))$ around the point $\widehat{x}$, with $S(u) = \mathbb{C}\nabla u^s$.

The boundary value problem (A.26) admits an explicit solution. For $p_i = 0$, its solution can be found in (Novotny and Sokołowski, 2013, Ch. 5, pp. 156), for instance. Since the stress $S_\varepsilon(w_\varepsilon)$ is uniform inside the inclusion, the solution of (A.26) for $p_i \neq 0$ can be written in a following compact form as

$$S_\varepsilon(w_\varepsilon)_{|_{B_\varepsilon}} = \mathbb{T}_\gamma S(u)(\widehat{x}) + \rho^{-1}\mathrm{T}_\gamma\,, \quad \text{(A.27)}$$

where $\mathbb{T}_\gamma$ is a fourth order isotropic tensor given by

$$\mathbb{T}_\gamma = \frac{\gamma(1-\gamma)}{2(1+\beta\gamma)}\left(2\beta\mathbb{I} + \frac{\alpha-\beta}{1+\alpha\gamma}\mathrm{I}\otimes\mathrm{I}\right) \quad \text{(A.28)}$$

and T_γ is a second order isotropic tensor written as

$$\mathrm{T}_\gamma = p_i\frac{\alpha\gamma}{1+\alpha\gamma}\mathrm{I}\,. \quad \text{(A.29)}$$

Note that by multiplying both sides of (A.27) by the parameter ρ we have

$$\sigma_\varepsilon(w_\varepsilon)_{|_{B_\varepsilon}} = \mathbb{T}_\gamma \sigma(u)(\widehat{x}) + \mathrm{T}_\gamma \ . \tag{A.30}$$

Remark 4. *The result shown in* (A.30) *fits the famous Eshelby problem. Formulated by Eshelby (1957, 1959), this problem plays a central role in the theory of elasticity involving the determination of effective elastic properties of materials with multiple inhomogeneities (inclusions, pores, defects, cracks, etc.). This important result represents one of the major advances in the continuum mechanics theory of the* 20^{th} *century (Kachanov et al., 2003).*

Now we can construct $\sigma_\varepsilon(\tilde{u}_\varepsilon)$ in such a way that it compensates for the discrepancies introduced by the higher-order terms in ε as well as by the boundary-layer w_ε on the exterior boundary $\partial\Omega$. It means that the remainder $\tilde{u}_\varepsilon$ must be solution to the following boundary value problem: Find $\tilde{u}_\varepsilon$ such that

$$\left\{\begin{array}{rcll} \mathrm{div}\sigma_\varepsilon(\tilde{u}_\varepsilon) &=& 0 & \text{in} \quad \Omega \ , \\ \sigma_\varepsilon(\tilde{u}_\varepsilon) &=& \gamma_\varepsilon \sigma(\tilde{u}_\varepsilon) \ , & \\ \tilde{u}_\varepsilon &=& g_1 & \text{on} \quad \partial\Omega \ , \\ \left.\begin{array}{rcl} [\![\tilde{u}_\varepsilon]\!] &=& 0 \\ [\![\sigma_\varepsilon(\tilde{u}_\varepsilon)]\!]\, n &=& g_2 \end{array}\right\} & & \text{on} \quad \partial\omega \ , \\ \left.\begin{array}{rcl} [\![\tilde{u}_\varepsilon]\!] &=& 0 \\ [\![\sigma_\varepsilon(\tilde{u}_\varepsilon)]\!]\, n &=& \varepsilon h \end{array}\right\} & & \text{on} \quad \partial B_\varepsilon \ , \end{array}\right. \tag{A.31}$$

where $g_1 = -w_\varepsilon$, $g_2 = -(1-\rho_0)S(w_\varepsilon)n$ and $h = (1-\gamma)(\nabla\sigma(u(\xi))n)n$, with ξ used to denote an intermediate point between x and $\widehat{x}$. The estimate $\|\tilde{u}_\varepsilon\|_{H^1(\Omega)} = O(\varepsilon^2)$ for the remainder $\tilde{u}_\varepsilon$ holds true. See, for instance, (Novotny and Sokołowski, 2013, Ch. 5, pp 155).

From the above results, we can evaluate the integrals in (A.24) explicitly. In fact, after replacing the ansätz for u_ε given by (A.25) in the first integral of (A.24) we have

$$\int_{B_\varepsilon} \sigma_\varepsilon(u_\varepsilon)\cdot\nabla u^s dx = \underbrace{\int_{B_\varepsilon} \sigma_\varepsilon(u)\cdot\nabla u^s \, dx}_{(a)} + \underbrace{\int_{B_\varepsilon} \sigma_\varepsilon(w_\varepsilon)\cdot\nabla u^s \, dx}_{(b)} + \mathcal{E}_1(\varepsilon) \ . \tag{A.32}$$

The remainder $\mathcal{E}_1(\varepsilon)$ is given by

$$\begin{aligned} \mathcal{E}_1(\varepsilon) &= \int_{B_\varepsilon} \sigma_\varepsilon(\tilde{u}_\varepsilon)\cdot\nabla u^s dx \\ &\leq \|\sigma_\varepsilon(\tilde{u}_\varepsilon)\|_{L^2(B_\varepsilon)} \|\nabla u\|_{L^2(B_\varepsilon)} \\ &\leq c_1 \|\tilde{u}_\varepsilon\|_{H^1(\Omega)} \|\nabla u\|_{L^2(B_\varepsilon)} \leq c_2\varepsilon^3 = O(\varepsilon^3) \ , \end{aligned} \tag{A.33}$$

where we have used the Cauchy-Schwarz inequality together with the estimation for the remainder $\tilde{u}_\varepsilon$. The term (a) in (A.32) can be developed in power of ε as follows

$$\begin{aligned} \int_{B_\varepsilon} \sigma_\varepsilon(u)\cdot\nabla u^s dx &= \int_{B_\varepsilon} \gamma\sigma(u)\cdot\nabla u^s dx \\ &= \pi\varepsilon^2 \gamma\sigma(u)(\hat{x})\cdot\nabla u^s(\hat{x}) + \mathcal{E}_2(\varepsilon) \ , \end{aligned} \tag{A.34}$$

with the remainder $\mathcal{E}_2(\varepsilon)$ defined as

$$\begin{aligned} \mathcal{E}_2(\varepsilon) &= \int_{B_\varepsilon} (h(x) - h(\hat{x}))dx \\ &\leq \|h(x) - h(\hat{x})\|_{L^2(B_\varepsilon)} \|1\|_{L^2(B_\varepsilon)} \\ &\leq c_1\varepsilon \|x - \hat{x}\|_{L^2(B_\varepsilon)} \leq c_2\varepsilon^3 = O(\varepsilon^3) \ , \end{aligned} \tag{A.35}$$

where we have introduced the notation

$$h(x) - h(\hat{x}) = \sigma(u)(x)\cdot\nabla u^s(x) - \sigma(u)(\hat{x})\cdot\nabla u^s(\hat{x}) \ . \tag{A.36}$$

Note that, we have used again the Cauchy-Schwarz inequality and the interior elliptic regularity of function u. Since the exact solution of the auxiliary problem (A.26) is known, the term (b) in (A.32) can be written as

$$\int_{B_\varepsilon} \sigma_\varepsilon(w_\varepsilon) \cdot \nabla u^s dx = \pi\varepsilon^2 \nabla u^s(\hat{x}) \cdot (\mathbb{T}_\gamma \sigma(u)(\hat{x}) + \mathrm{T}_\gamma) + \mathcal{E}_3(\varepsilon) \ . \tag{A.37}$$

The remainder $\mathcal{E}_3(\varepsilon)$ is given by

$$\begin{aligned} \mathcal{E}_3(\varepsilon) &= \int_{B_\varepsilon} \sigma_\varepsilon(w_\varepsilon) \cdot (\nabla u^s - \nabla u^s(\hat{x})) dx \\ &\leq \|\sigma_\varepsilon(w_\varepsilon)\|_{L^2(B_\varepsilon)} \|\nabla u - \nabla u(\hat{x})\|_{L^2(B_\varepsilon)} \\ &\leq c_1 \varepsilon \|x - \hat{x}\|_{L^2(B_\varepsilon)} \leq c_2 \varepsilon^3 = O(\varepsilon^3) \ , \end{aligned} \tag{A.38}$$

where we have used again the Cauchy-Schwarz inequality and the interior elliptic regularity of function u.

The second term in (A.24) can be developed as follows

$$\int_{B_\varepsilon} p_i \, \mathrm{div}(u) dx = \pi\varepsilon^2 p_i \, \mathrm{div}(u)(\hat{x}) + \mathcal{E}_4(\varepsilon) \ , \tag{A.39}$$

where the remainder $\mathcal{E}_4(\varepsilon)$ is defined as

$$\begin{aligned} \mathcal{E}_4(\varepsilon) &= \int_{B_\varepsilon} p_i (\mathrm{div}(u) - \mathrm{div}(u)(\hat{x})) dx \\ &\leq c_1 \|x - \hat{x}\|_{L^2(B_\varepsilon)} \|1\|_{L^2(B_\varepsilon)} \leq c_2 \varepsilon^3 = O(\varepsilon^3) \ . \end{aligned} \tag{A.40}$$

Once again, we have used the Cauchy-Schwartz inequality together with the interior elliptic regularity of function u.

After replacing the ansätz for u_ε given by (A.25) into the last term of (A.24) we have

$$\frac{1}{2} \int_{B_\varepsilon} p_i \, \mathrm{div}(u_\varepsilon - u) dx = \frac{1}{2} \int_{B_\varepsilon} p_i \, \mathrm{div}(w_\varepsilon + \tilde{u}_\varepsilon) dx = \frac{1}{2} \int_{B_\varepsilon} p_i \, \mathrm{div}(w_\varepsilon) dx + \mathcal{E}_5(\varepsilon) \ . \tag{A.41}$$

where the remainder $\mathcal{E}_5(\varepsilon)$ has the following bound thanks to the estimate for $\tilde{u}_\varepsilon$

$$\begin{aligned} \mathcal{E}_5(\varepsilon) &= \frac{1}{2} \int_{B_\varepsilon} p_i \, \mathrm{div}(\tilde{u}_\varepsilon) dx \\ &\leq c_1 \|\nabla \tilde{u}_\varepsilon\|_{L^2(B_\varepsilon)} \|1\|_{L^2(B_\varepsilon)} \\ &\leq c_2 \varepsilon \|\tilde{u}_\varepsilon\|_{H^1(\Omega)} \leq c_2 \varepsilon^3 = O(\varepsilon^3) \ . \end{aligned} \tag{A.42}$$

By using the constitutive relation and after algebraic manipulations, we have

$$\frac{1}{2} \int_{B_\varepsilon} p_i \, \mathrm{div}(w_\varepsilon) dx = \frac{1}{2} \int_{B_\varepsilon} \frac{p_i}{2\gamma\rho(\mu + \lambda)} \mathrm{tr}\sigma_\varepsilon(w_\varepsilon) dx \ , \tag{A.43}$$

where $\mathrm{tr}\sigma_\varepsilon(w_\varepsilon)$, evaluated inside the inclusion, is given by

$$\mathrm{tr}\sigma_\varepsilon(w_\varepsilon)_{|_{B_\varepsilon(\hat{x})}} = \frac{\alpha\gamma}{1 + \alpha\gamma} ((1 - \gamma)\mathrm{tr}\sigma(u)(\hat{x}) + 2p_i) \ . \tag{A.44}$$

From the above results, the variation of the energy shape functionals, given by (A.24), can be developed in power of ε as follows

$$\begin{aligned}\mathcal{J}_{\chi_\varepsilon}(u_\varepsilon) - \mathcal{J}(u) = &- \pi\varepsilon^2 \frac{1-\gamma}{2\gamma}\left[\gamma\sigma(u)(\hat{x}) + (\mathbb{T}_\gamma\sigma(u)(\hat{x}) + \mathrm{T}_\gamma)\right]\cdot\nabla u^s(\hat{x}) \\ &- \pi\varepsilon^2 p_i \operatorname{div}(u)(\hat{x}) - \pi\varepsilon^2 \frac{\alpha}{2}\frac{1-\gamma}{1+\alpha\gamma} p_i \operatorname{div}(u)(\hat{x}) \\ &- \pi\varepsilon^2 \frac{p_i^2}{2\mu\rho(1+\alpha\gamma)} + \sum_{i=1}^{5}\mathcal{E}_i(\varepsilon)\ , \end{aligned} \tag{A.45}$$

where the remainders $\mathcal{E}_i(\varepsilon) = o(\varepsilon^2)$, for $i = 1, ..., 5$, as previously shown. By defining the function $f(\varepsilon) = \pi\varepsilon^2$ and after applying the topological derivative concept in (A.45), we obtain

$$D_T\mathcal{J}(\hat{x}) = -\mathbb{P}_\gamma\sigma(u)(\hat{x})\cdot\nabla u^s(\hat{x}) - \frac{1+\alpha}{1+\alpha\gamma} p_i \operatorname{div}(u)(\hat{x}) - \frac{1}{2\rho\mu}\frac{p_i^2}{(1+\alpha\gamma)}\ , \tag{A.46}$$

where $\mathbb{P}_\gamma$ is a fourth order isotropic tensor given by

$$\mathbb{P}_\gamma = \frac{1}{2}\frac{1-\gamma}{1+\beta\gamma}\left((1+\beta)\mathbb{I} + \frac{1}{2}(\alpha-\beta)\frac{1-\gamma}{1+\alpha\gamma}\mathrm{I}\otimes\mathrm{I}\right)\ , \tag{A.47}$$

with the coefficients α and β defined as

$$\alpha = \frac{\lambda+\mu}{\mu} \quad \text{and} \quad \beta = \frac{\lambda+3\mu}{\lambda+\mu}\ . \tag{A.48}$$

For more details concerning the polarization tensor (A.47), see for instance the book by Ammari and Kang (2007).

References

G. Allaire, F. Jouve, and N. Van Goethem. Damage and fracture evolution in brittle materials by shape optimization methods. *Journal of Computational Physics*, 230(12): 5010–5044, 2011.

H. Ammari and H. Kang. *Polarization and moment tensors with applications to inverse problems and effective medium theory*. Applied Mathematical Sciences vol. 162. Springer-Verlag, New York, 2007.

B. Bourdin, G. A. Francfort, and J. J. Marigo. Numerical experiments in revisited brittle fracture. *Journal of the Mechanics and Physics of Solids*, 48(4):797–826, 2000.

B. Bourdin, G. A. Francfort, and J. J. Marigo. The variational approach to fracture. *Journal of Elasticity*, 91(1-3):5–148, 2008.

T. D. Cao, E. Milanese, E. W. Remij, P. Rizzato, J. J. C. Remmers, L. Simoni, J. M. Huyghe, F. Hussain, and B. A. Schrefler. Interaction between crack tip advancement and fluid flow in fracturing saturated porous media. *Mechanics Research Communications*, 80:24–37, 2017.

J. D. Eshelby. The determination of the elastic field of an ellipsoidal inclusion, and related problems. *Proceedings of the Royal Society: Section A*, 241:376–396, 1957.

J. D. Eshelby. The elastic field outside an ellipsoidal inclusion, and related problems. *Proceedings of the Royal Society: Section A*, 252:561–569, 1959.

Y. Feng and K. E. Gray. Parameters controlling pressure and fracture behaviors in field injectivity tests: A numerical investigation using coupled flow and geomechanics model. *Computers and Geotechnics*, 87:49–61, 2017.

G. A. Francfort and J. J. Marigo. Stable damage evolution in a brittle continuous medium. *European Journal of Mechanics, A/Solids*, 12(2):149–189, 1993.

S. M. Giusti, A. Ferrer, and J. Oliver. Topological sensitivity analysis in heterogeneous anisotropic elasticity problem. theoretical and computational aspects. *Computer Methods in Applied Mechanics and Engineering*, 311:134–150, 2016.

M. Kachanov, B. Shafiro, and I. Tsukrov. *Handbook of Elasticity Solutions*. Kluwer Academic Publishers, Dordrecht, 2003.

J. Kim and G. J. Moridis. Numerical analysis of fracture propagation during hydraulic fracturing operations in shale gas systems. *International Journal of Rock Mechanics & Mining Sciences*, 76:127–137, 2015.

T. P. L'homme, C. J. de Pater, and P. H. Helfferich. Experimental study of hydraulic fracture initiation in colton sandstone. *Society of Petroleum Engineers*, 2002.

E. Milanese, O. Yilmaz, J. F. Molinari, and B. A. Schrefler. Avalanches in dry and saturated disordered media at fracture. *Physical Review E*, 93:043002, 2016.

A. A. Novotny and J. Sokołowski. *Topological derivatives in shape optimization*. Interaction of Mechanics and Mathematics. Springer-Verlag, Berlin, Heidelberg, 2013.

L. C. Pereira, L. J. N. Guimarães, B. Horowitz, and M. Sánchez. Coupled hydro-mechanical fault reactivation analysis incorporating evidence theory for uncertainty quantification. *Computers and Geotechnics*, 56:202–215, 2014.

S. Salimzadeh, A. Paluszny, and R. W. Zimmerman. Three-dimensional poroelastic effects during hydraulic fracturing in permeable rocks. *International Journal of Solids and Structures*, 108:153–163, 2017.

S. Secchi and B. A. Schrefler. A method for 3-d hydraulic fracturing simulation. *International Journal of Fracture*, 178(1):245–258, 2012.

J. Sokołowski and A. Żochowski. On the topological derivative in shape optimization. *SIAM Journal on Control and Optimization*, 37(4):1251–1272, 1999.

M. Y. Soliman, M. Wigwe, A. Alzahabi, E. Pirayesh, and N. Stegent. Analysis of fracturing pressure data in heterogeneous shale formations. *Hydraulic Fracturing Journal*, 1(2): 8–12, 2014.

N. Van Goethem and A. A. Novotny. Crack nucleation sensitivity analysis. *Mathematical Methods in the Applied Sciences*, 33(16):1978–1994, 2010.

M. Xavier and A. A. Novotny. Topological derivative-based topology optimization of structures subject to design-dependent hydrostatic pressure loading. *Structural and Multidisciplinary Optimization*, 56(1):47–57, 2017.

M. Xavier, E. A. Fancello, J. M. C. Farias, N. Van Goethem, and A. A. Novotny. Topological derivative-based fracture modelling in brittle materials: A phenomenological approach. *Engineering Fracture Mechanics*, 179:13–27, 2017.

G. Q. Zhang and M. Chen. Dynamic fracture propagation in hydraulic re-fracturing. *Journal of Petroleum Science and Engineering*, 70:266–272, 2010.

(M. Xavier and A.A. Novotny) Laboratório Nacional de Computação Científica LNCC/MCT, Coordenação de Matemática Aplicada e Computacional, Av. Getúlio Vargas 333, 25651-075 Petrópolis - RJ, Brasil

E-mail address: {marcel,novotny}@lncc.br

(N. Van Goethem) Universidade de Lisboa, Faculdade de Ciências, Departamento de Matemática, CMAF+CIO, Alameda da Universidade, C6, 1749-016 Lisboa, Portugal

E-mail address: vangoeth@fc.ul.pt